

# Spin wave resonance in yttrium iron garnet stripe domains

Daniel Prestwood,<sup>1,2,3,\*</sup> Chris Barker,<sup>4</sup> Kilian D. Stenning,<sup>3</sup> Charlie W. F. Freeman,<sup>1,2,4</sup> Tianyi Wei,<sup>1,2</sup> Takashi Kikkawa,<sup>5,6</sup> Troy Dion,<sup>7</sup> Daniel Stoeffler,<sup>8</sup> Yves Henry,<sup>8</sup> Matthieu Bailluel,<sup>8</sup> Noora Naushad,<sup>9</sup> William Griggs,<sup>9</sup> Thomas Thomson,<sup>9</sup> Murat Cubukcu,<sup>1,4</sup> Jack C. Gartside,<sup>3,10</sup> Eiji Saitoh,<sup>6,11,12,13</sup> Will R. Branford,<sup>3,10</sup> and Hidekazu Kurebayashi<sup>1,2,13</sup>

<sup>1</sup>*London Centre for Nanotechnology, University College London,  
London, WC1H 0AH, United Kingdom*

<sup>2</sup>*Department of Electronic and Electrical Engineering, University College London,  
London, WC1E 7JE, United Kingdom*

<sup>3</sup>*Blackett Laboratory, Imperial College London, London SW7 2AZ, United Kingdom*

<sup>4</sup>*National Physics Laboratory, Hampton Rd, Teddington TW11 0LW, United Kingdom*

<sup>5</sup>*Advanced Science Research Center, Japan Atomic Energy Agency, Tokai 319-1195, Japan*

<sup>6</sup>*Department of Applied Physics, The University of Tokyo, Tokyo 113-8656, Japan*

<sup>7</sup>*Solid State Physics Laboratory, Kyushu University, Japan*

<sup>8</sup>*Université de Strasbourg, CNRS, Institut de Physique et Chimie des Matériaux de Strasbourg,  
UMR 7504, F-67000 Strasbourg, France*

<sup>9</sup>*NEST Research Group, Department of Computer Science, The University of Manchester, Oxford Road,  
Manchester, M13 9PL, United Kingdom*

<sup>10</sup>*London Centre for Nanotechnology, Imperial College London,  
London, SW7 2AZ, United Kingdom*

<sup>11</sup>*Institute for AI and Beyond, The University of Tokyo, Tokyo 113-8656, Japan*

<sup>12</sup>*RIKEN Center for Emergent Matter Science (CEMS), Wako 351-0198, Japan*

<sup>13</sup>*WPI-Advanced Institute for Materials Research, Tohoku University, Sendai 980-8577, Japan*  
(Dated: May 14, 2025)

We study a thin film yttrium iron garnet sample that exhibits magnetic stripe domains due to a small perpendicular magnetic anisotropy. Using wide-field magneto-optic Kerr effect measurements we reveal the domain pattern evolution as a function of applied field and discuss the role of the cubic anisotropy for the domain formation. Rich magnetic resonant spectra for the stripe domain background are observed for different excitation conditions and micromagnetic simulations provide spatial profiles of each resonance mode. We further simulate domain patterns and resonance spectra as a function of the cubic anisotropy to correlate between them. This study highlights magnetic domain structures to host complex resonant behaviour in a low-damping magnetic material, for a potential use of future applications in magnonics.

## I. INTRODUCTION

Yttrium iron garnet (YIG) is a widely used material within the field of spintronics [1] and magnonics [2–4] due to its low intrinsic damping (Gilbert damping constant  $\alpha$  down to  $5 \times 10^{-5}$  [5]). For magnonic applications, YIG is typically studied in the collinear saturated magnetic state where the macrospin picture is effective to describe its spin-wave properties [6–10]. Non uniform magnetic textures such as stripe, helical and vortex states, have been shown to display rich dynamic properties and ability to host multiple resonant modes of varied character [11–15]. Spinwave excitation in systems of varying non-collinear magnetization textures have been exploited for demonstrating unconventional computing applications e.g. reservoir computing [13, 16–19]

Fabrication of YIG for magnonic devices often requires etching which may lead to surface damage and reduction in material quality, such as enhancing damping [20]. Other techniques such as laser heating [21] and ion beam

irradiation [22] still present the inflexibility of making irreversible changes to the physical properties. On the other hands, magnetic domain structures naturally offer a route to reconfigurably altering spin wave spectra and propagation without permanently altering material shape or parameters [23, 24]. For example, domain walls can act as nano-channels to guide spin waves [25–27] or as local spin wave emitters [28–30].

Micromagnetic domain patterns result from minimizing local energetics depending on factors such as magnetic anisotropy, magnetic dipole interaction and applied field. High perpendicular magnetic anisotropy (PMA) materials often exhibit stripes, labyrinths and bubble domains [31], whereas materials with cubic anisotropy host Landau and fractal patterns in order to reduce the closure energy [32]. Stripe domains are commonly found in thin films with small PMA [33–35] which in this context refers to a quality factor,  $Q$ , of less than 1, where  $Q = 2K_{\perp}/\mu_0 M_s^2$  with  $K_{\perp}$  being the uniaxial anisotropy constant and  $M_s$  the saturation magnetisation [32]. These stripes can exist at zero external field when the film thickness is above the critical thickness,  $D_{\text{cr}} = 2\pi\sqrt{A/K_{\perp}}$  where  $A$  is the exchange stiffness. For thicker films a Landau structure of flux closure domains

\* daniel.prestwood.22@ucl.ac.uk

can form at the film surface in order to reduce the surface energy [32].

Resonant properties of the stripe domain state have been studied on several occasions in substituted YIG [36–38] and others [35, 39–41]. These studies often show multiple resonant modes in domains and domain-walls, in thicker films, characteristic modes of flux closure caps [39]. A previous study of the propagation of magneto-statics waves in stripe domain YIG [42] found that the different domain states could offer varying modes of propagation with a limited amount of theoretical and numerical analysis using a microspin model.

In this study, we characterised both static and dynamic properties of 3  $\mu\text{m}$  thick YIG thin films. For the dynamic properties we concern ourselves primarily with the standing wave modes that are set up in the cross section of the stripe domain pattern. We observe how this regime is predisposed to mode hybridisation due to the confined nature and varying trajectories these modes. Micromagnetic simulations provide spinwave spectra that agree well with our observations, allowing us to map out of the spatial distribution of the various resonant modes within different regions of the magnetic domain pattern.

## II. RESULTS

### A. Stripe domain formation

The YIG crystal studied is a 3  $\mu\text{m}$  thin film grown on a [111]-oriented gadolinium gallium garnet (GGG) substrate using liquid phase epitaxy (LPE) [43, 44] as illustrated in Fig. 1(a). The PMA in the sample, measured to be approximately  $1600 \text{ Jm}^{-3}$  (providing a  $Q$  value of 0.12) led to the formation of stripe domains as confirmed by magneto-optic Kerr effect (MOKE) images shown in Fig. 1(b). Although the crystal structure of YIG does not allow any intrinsic uniaxial anisotropy, PMA in thin films can potentially arise from the inversion-breaking at the surface and tetragonal distortion due to growth-induced strain [45]. The thickness of our YIG sample makes surface effects an unlikely explanation. Growth-induced anisotropy has previously been observed in [111] YIG in [46] and [47] where the GGG substrate was polished away to remove the contribution of stress.

We begin by examining the remanent magnetisation state after saturating along various in-plane angles from the  $\langle 110 \rangle$  direction (see Fig. 1(a)). During this process, the sample becomes fully magnetised and once the field is taken off, the stripe domain state forms. As shown in Fig. 1(b), for the easy axis orientations (0 and 60 degrees), co-linear magnetic stripe domains are observed, whereas along the hard axes, a ‘chevron’ pattern emerges, revealing its in-plane six-fold nature consistent with the symmetry of the (111) plane. We have observed that stripe realignment also occurs for applied fields below saturation. As such, in all our experiments, a sufficiently large field is applied to align the stripe domains prior to

measurement.

To further understand the evolution of stripe domains, we imaged the magnetisation state in an external field applied along the  $[1\bar{1}0]$  and  $[11\bar{2}]$  axis. The field evolution of the stripes when applied along the  $[1\bar{1}0]$  axis is shown in Fig. 1(c). In this direction, changes with a field increase are relatively uneventful, only showing a gradual increase of the stripe periodicity prior to domain disappearance - see the reciprocal mapping of Fig. 1(e). In contrast, the domain evolution for fields applied along the  $[11\bar{2}]$  axis displays more dramatic changes as shown in Fig. 1(d). The stripes originate in the ‘chevron’ state which quickly gives way to the collinear stripes at a relatively low field before somewhat surprisingly returning to the ‘chevron’ state at 3 mT. After this, the domains straighten along the field axis. The periodicity of the stripe domains increases before eventually saturating at  $\approx 5.5 \text{ mT}$  as more precisely recognised in Fig. 1(f) which shows the wave vector reduction along the  $[1\bar{1}0]$  direction. We can also identify the chevron state via the broadening in reciprocal space along the x-axis showing a finite periodicity in this direction. While there is a gradual transition from the collinear state to the ‘chevron’ state, the transition from the chevron state to collinear at greater field is much more abrupt. Our observation is consistent with previous work for [111] oriented YIG [42, 48], although the chevron state was not present in zero field. The easy and hard axis behaviour are representative of coherent rotation and domain propagation magnetisation processes, respectively.

To explain the observed phenomena, we employ micromagnetic simulations (mumax3) [49]. Figure 2(a) shows a vertical section of the thin film with the height of the simulation set to the film thickness and the width to the stripe period. Periodic boundary conditions were then used to ensure a realistic demagnetising field. As shown in Fig. 2b, stripe domains are successfully reproduced as the equilibrium state after removing the field, consistent with our MOKE observation. Flux closure domains are present at the top and bottom surfaces, characteristic of thicker films [32, 50]. Applying a field along the  $[1\bar{1}0]$  and  $[11\bar{2}]$  directions produces results that agree well with the MOKE images in Fig. 1. In these simulations, the field is applied out of the plane (equivalent to in-plane in the experiment) and as such along the stripe direction.

Figure 2(c) shows that the increasing periodicity of the stripes by the in-plane field is reproduced in the  $[11\bar{2}]$  simulation. For the  $[1\bar{1}0]$  case, we are able to observe a behaviour not elucidated by MOKE, i.e. a slanting of the stripe domains under the applied field (Fig. 2(d)). Figures 2(e-f) show the measured and simulated magnetisation loops for the two different axes. The general shape of these matches well with a small hysteresis in the centre of the loop due to magnetisation switching within the domain walls. One visible disagreement is that the width of hystereses in the simulation is larger than those in experiments, as is the saturation field. We speculate that this is due to the inaccuracy in reproducing the en-

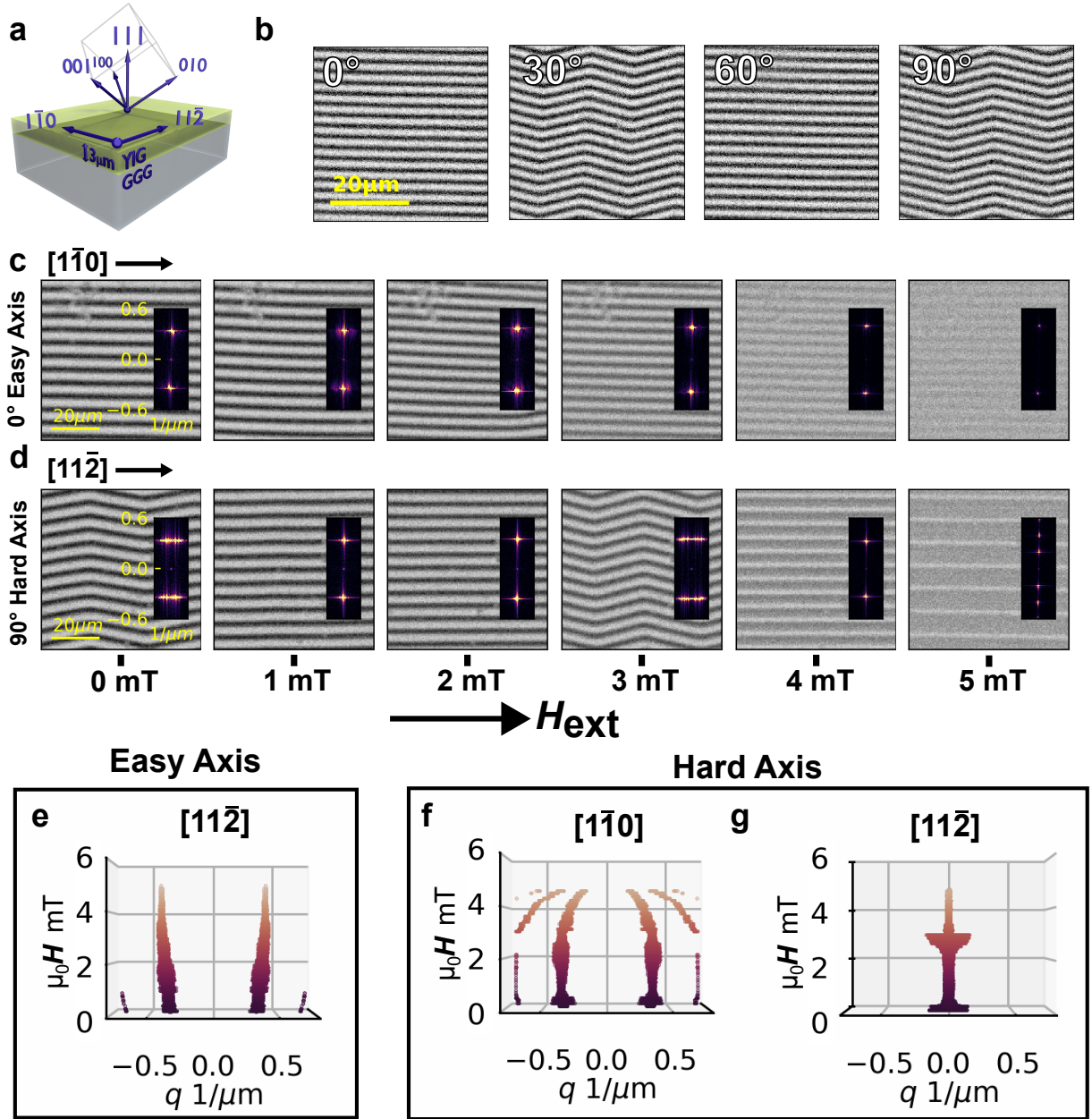


FIG. 1. (a) Diagram of the YIG sample with labelled crystalline axes. (b) Wide field Kerr images of magnetisation state at remanence after saturating an external field of 17mT at 0, 30, 60 and 90 degrees w.r.t the easy axis. c,d) Field evolution of the magnetic state for the field being applied along either hard axis (c) or easy axis (d). Inset shows the Fourier transform of each image. Position of Fourier transform peaks as a function of the applied field for easy axis (e) and hard axis (f-g). For easy axis, we see a smooth change from stripe to saturated consistent with a coherent rotation magnetisation process, whereas for the hard axis, we see a transition into a state where one set of domains expand while the others shrink a process which is consistent with a domain propagation magnetisation process.

ergy of the magnetic dipole interaction which determines the domain-wall energy and its switching fields, due to the limited spatial boundary conditions for our simulations - further discussions can be found in Appendix A. The qualitative agreement lead us to use these simulation parameters in the present study.

This behaviour can be explained by examining the first order cubic anisotropy energy density (Fig. 2(g) which is given by the following [51]:

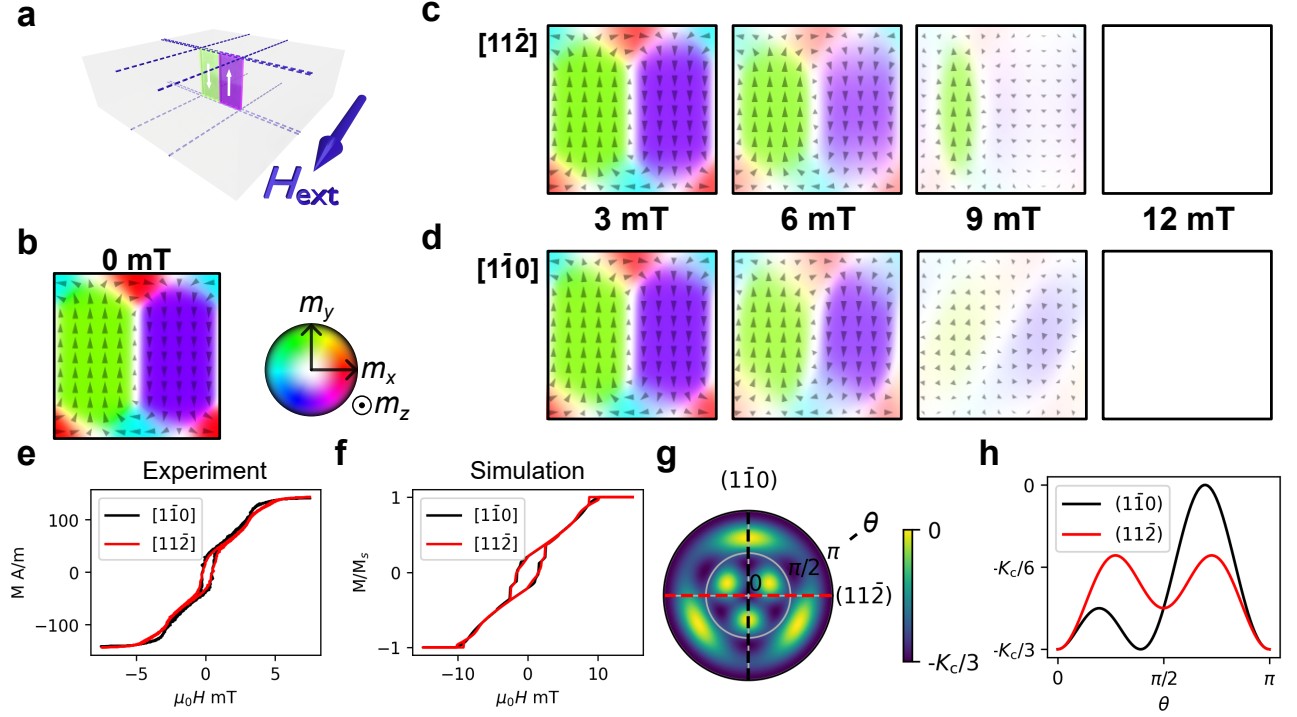


FIG. 2. Simulation of the remnant state of the simulation (a). With the micromagnetic state for increasing field along the  $[1\bar{1}0]$  (b) and  $[11\bar{2}]$  (c) axes. (d) Schematic showing the simulation geometry. Measured (e) and simulated (f) magnetisation loops for both the  $[1\bar{1}0]$  and  $[11\bar{2}]$  axes.

$$E = K_c \left( \frac{\sin^4 \theta}{4} + \sqrt{2} \cos^2 \phi \cos \theta \sin \phi \sin^3 \theta + \frac{\cos^4 \theta}{3} + \frac{\sqrt{2} \cos \theta \sin^3 \phi \sin^3 \theta}{3} \right) \quad (2)$$

Where  $\theta$  is the polar angle from the  $[111]$  direction and  $\phi$  is the azimuthal angle in the  $(111)$  plane such that  $\phi = 0$  points along the  $[1\bar{1}0]$  direction. The three hard axes directed along the  $\langle 100 \rangle$  directions. Using this we can examine three important case the energy density for the plane perpendicular to the  $[111]$  direction (i.e. the plane that defines the measured thin film) is equipotential within the plane expressed as  $E_{\perp[111]} = K_c/4$ . As such, there is no hard or easy axis within the plane. We however chose to refer to the  $[11\bar{2}]$  as the hard axis since we observe that the stripes prefer not to align along this axis in zero field (seen in Fig.1(d)) while for the  $[1\bar{1}0]$  axis they do (Fig.1(c)) as an easy axis behaviour.

We can also calculate the energy density as a function of polar angle from the  $[111]$  direction in the  $(11\bar{2})$  (containing the  $[1\bar{1}0]$  direction) and  $(1\bar{1}0)$  (containing the  $[11\bar{2}]$  direction) planes as follows:

$$E_{(1\bar{1}0)} = K_c \left( \frac{\cos^4 \theta}{3} + \frac{\sqrt{2} \cos \theta \sin^3 \theta}{9} + \frac{\sin^4 \theta}{4} \right) \quad (1)$$

From this we can observe that  $E_{(1\bar{1}0)}$  has a term that is odd in  $\theta$  around the in-plane direction,  $\theta = \pi/2$  (Fig. 2(h)). As such, when  $\mathbf{H}_{\text{ext}}$  is applied along the  $[11\bar{2}]$  and the two stripes begin to magnetize into the plane of the film one stripe will approach a maxima of the anisotropy energy while the other approaches an energy minima. This is what leads to one set of stripes expanding while the other shrinks. Conversely, when magnetising along the  $[1\bar{1}0]$  direction we can see that  $E_{(11\bar{2})}$  is completely even in  $\theta$  (Fig. 2(h)) and as such neither stripe is favoured. By more closely examining the energy density (Fig. 2(g)) we can also see that as the stripe is magnetising into the film plane it becomes energetically favourable for the magnetisation of the stripes to tilt slightly explaining the behaviour close to saturation seen in the simulations.

## B. Stripe domain resonances

We performed microwave absorption experiments by placing the YIG sample on a broadband waveguide. Excited spinwave modes as a function of frequency and applied magnetic field are measured by the transmission coefficient  $S_{12}$  using a vector network analyser - here the end of the waveguide is open-circuited for full reflection.



We apply external dc magnetic field both perpendicular and parallel to the oscillating magnetic field, so-called perpendicular and parallel pumping geometry, to capture all the modes excited in the unsaturated regime. We repeat the same experiments after rotating the sample by 90 degrees in-plane. While in simulation the stripes are aligned along the the field direction by design, in the experiment we apply an initial saturating field prior to each scan to ensure that the stripes are aligned along the field direction. It should be noted that since the sample is laterally larger than the signal line, an out of plane (OOP) component of the RF excitation for both pumping regimes is present in the YIG sample. Furthermore, because the width of the signal line is large (0.5 mm), the wavelength of excited spinwave modes is practically indistinguishable to that of the uniform mode.

Figure 3 presents spinwave spectra and simulation results for the perpendicular pumping with  $\mathbf{H}_{\text{ext}}$  applied along the easy axis Fig. 3(a). The experimentally measured spectra as a function of field in Fig. 3(b) can be divided into three regimes. A low-field regime for 0 - 3.5 mT has clear stripe domain mainly polarised along the OOP directions; there is an intermediate field regime (3.5 - 6 mT) is associated with a slanting of the stripe domains along towards on the three anisotropy axes, according to our simulations; finally the moments are collinear to the applied field in the high-field regime ( $> 6$  mT) where the Kittel modes are present. Using the same parameters as used for the prior static simulations, we calculated the resonant spectra which reproduce some of the modes observed experimentally, as shown in Fig. 3(c). Three modes labelled as 1-3 on Fig. 3(c) are identifiable in the experimental spectra in a very similar frequency region. Their spatial power maps in Fig. 3(d) reveal that the lowest mode (Mode 1) is the domain wall mode associated with the  $90^\circ$  domain walls between the stripe domains and flux closure caps. Mode 2 has strong resonance at the top and bottom surfaces of the bulk stripe domains which have a tilted magnetisation from the bulk moments. Compared to the first two, Mode 3 is a bulk mode of the stripe domains themselves. The phase maps shown for the bulk mode (3) reveal the two stripe domains to be in phase along the  $x$ -axis but out of phase along the  $z$ , this being in the direction of the applied field. This phase relationship is indicative an acoustic mode as we would expect for the direction of the rf field being applied here. This characteristic is true for all the modes excited under this rf direction.

Modes resonating at a higher frequency than Mode 1-3 show a more hybridised character. This is apparent in the spatial mapping of the example mode shown from region 4 in Fig. 3(d) where high-order bulk modes resonate together with modes located in the flux closure domains. In general the modes in this region are characterised by a finite wave vector parallel to the magnetisation within the stripes. The modes in regions 4-6 are hybridised to the point where analysing individual modes does not offer much insight into the dynamics. However, picking out

general trends in these regions can allow us to understand the same spectral features that are also observed in experiment. The two modes from regions 5 and 6 that meet at saturation can be also be identified in the experiment. The power maps reveal these modes in these regions are the surface (5) and volume (6) modes.

Figure 4 shows spinwave spectra for the parallel pumping configuration and corresponding micromagnetic simulation results for  $\mathbf{H}_{\text{ext}}$  along the easy axis. Here we can also pick out modes 1 and 2 are localized to the same regions as modes 1 and 2 from the perpendicular pumping results, the difference in field frequency profile is likely explained by the different rf field direction leading to a different phase relationship between the stripes (Fig. 4(d)). The slight difference in the power maps for these modes also indicate a different hybridisations. Interestingly these modes primarily associated with the domain walls are not excited efficiently at lower fields for parallel pumping. This can be explained by the fact that magnetization in these regions is predominantly parallel to the rf field applied. This does not change as larger fields are applied suggesting that the hybridization with other modes is what allows these regions to be excited. Once again here for the higher frequency modes we use the shaded regions approach to discuss the resonant dynamics due to the degree of hybridisation we observe.

The modes in region 3 are predominantly characterised by excitation within the flux closure domains. Moving up higher frequencies in the region 4, their spatial power distributions reveal that the edge modes start to hybridise to the high-order bulk modes inside of domains. Modes in region 5 displays resonance mainly in the  $90^\circ$  domain walls, whereas those in region 6 are associated with the bulk domain modes having a two-dimensional standing-wave nature along the parallel and perpendicular to the thickness direction, coupled to the edge modes.

By following mode 1 to the high field regime where we see a discontinuous change in the resonant modes, which we label this mode 7, we can attempt to understand the intermediate phase that we see in our experiment. As we discussed earlier Fig 2(d) shows how before saturation the stripe domains pick up a magnetisation in-plane perpendicular to the applied field, simultaneously the cross section of the stripes also slants in the same direction. As is evident from the the power map of mode 7 in Fig 4 the slanting causes the direction of the  $k$ -vector of these spin waves to also slant in this direction and as such increasing the wavelength of the first order mode in tandem with any other higher order modes.

Moving on, we turn to the case where  $\mathbf{H}_{\text{ext}}$  is applied along the hard axis, which is summarised in Fig. 5 that displays difference in spectra, particularly in the intermediate-field region. We attribute this to the evolution of static magnetic states, i.e. for the easy axis we observed a slanting of the stripes away from the perpendicular direction as we increased magnetic field, while for the hard axis a expansion of one set of stripes along side the shrinking of the other occurs. This ground-

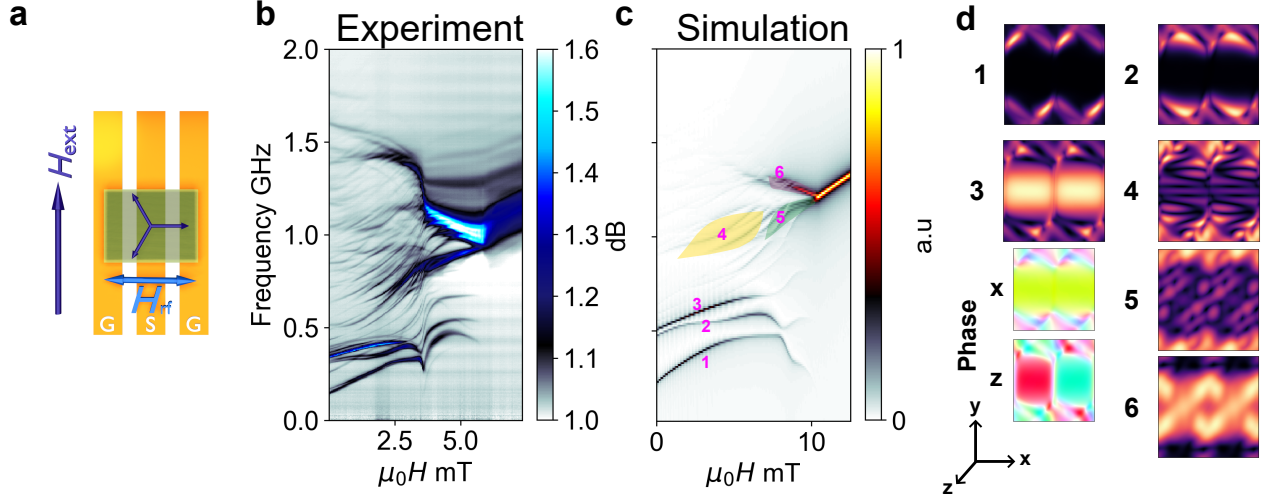


FIG. 3. a) Diagram showing the relative directions of external field, rf field and anisotropy axes. (b,c) Measured (b) and simulated (c) magnetic resonance spectra for YIG sample for  $\text{rf} \perp \mathbf{H}_{\text{ext}}$  which is directed along the  $[1\bar{1}0]$  axis. (d) power maps of spin wave modes labelled on (b) with a phase map shown for the bulk mode (3). The  $x$  and  $z$  axis are directed horizontally and out of the page respectively. With the  $z$  direction being along the axis of the stripe domains and the magnetisation within the stripes pointing along the  $y$  axis at zero field.

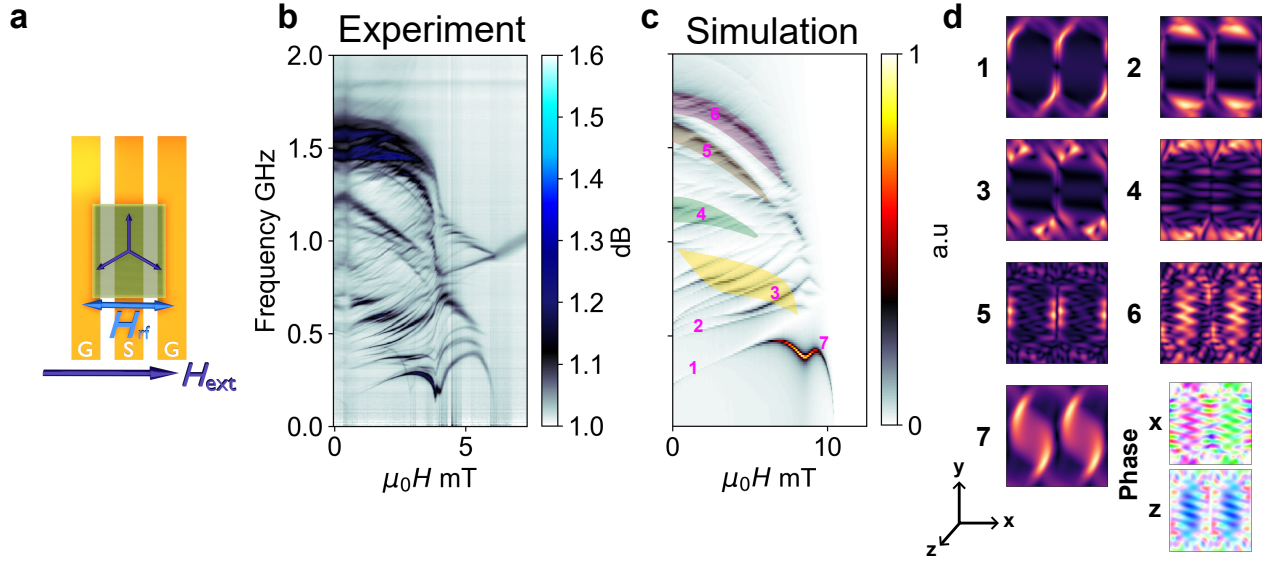


FIG. 4. a) Diagram showing the relative directions of external field, rf field and anisotropy axes. (b,c) Measured (b) and simulated (c) magnetic resonance spectra for YIG sample for  $\text{rf} \parallel \mathbf{H}_{\text{ext}}$  which is directed along the  $[1\bar{1}0]$  axis. (d) power maps of spin wave modes labelled on (c) with a phase map shown for the bulk mode (6).

state difference impacts on the resonant spectra for the intermediate-field regime (3.5 mT - 5 mT in experiment and 7 mT - 10 mT in simulation), together with noticeable difference in the low-field regime below 3.5 mT. The most notable feature is the energy splitting of the two stripes for the low frequency modes (Modes 1 and 2 and modes 3 and 4 in Fig. 5(d)) which share the same relative localisation within each stripe. The power maps in Fig. 5(d) reveal modes 1 and 2 to be domain wall modes but relating to different stripes magnetization. Mode 2

, active in domain walls of stripe magnetised positively along the OOP direction, has slightly higher energy than mode 1, which is associated with the stripe magnetised negatively OOP. Modes 6, 7 and those in region 8 reveal something about how the intermediate state where we observe uneven widths of the stripe domains affects the resonant spectra. Mode 6, like modes 1 and 2, is predominantly excited in the domain wall. However, in contrast to modes 1 and 2 this is localised to what would be the  $180^\circ$ , though, the magnetisation within the domains is

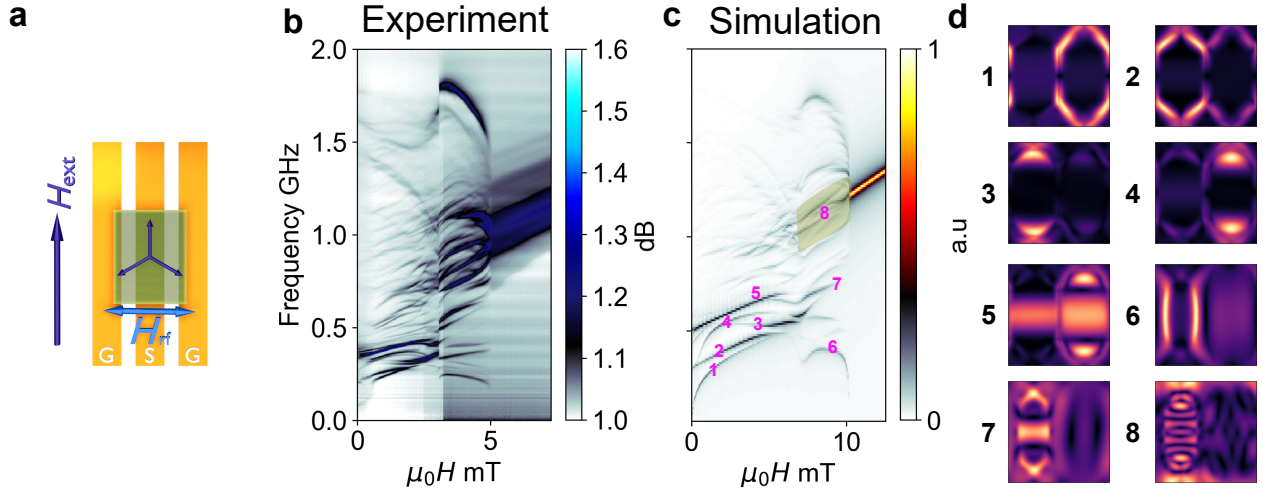


FIG. 5. a) Diagram showing the relative directions of external field, rf field and anisotropy axes. (b,c) Measured (b) and simulated (c) magnetic resonance spectra for YIG sample for  $\text{rf} \perp \mathbf{H}_{\text{ext}}$  which is directed along the  $[11\bar{2}]$  axis. (d) power maps of spin wave modes labelled on (c)

closer to having a  $90^\circ$  difference than  $180^\circ$ . The complex configuration of dipolar fields in this state make specific analysis of the character of the modes non-trivial but certainly the change in domain with in this region alters the wavelength of the standing wave modes with a  $k$ -vector directed across the domains. We see the reverse for modes 3 and 4 where the negatively magnetised stripe has a higher energy for this mode.

Finally, we show the last experimental geometry for the parallel pumping with  $\mathbf{H}_{\text{ext}}$  along the hard axis Fig. 6. The same energy splitting of the lower frequency modes is present and the shaded regions 5-8 appear to follow the same trend as those seen in Fig. 4(c). We also see a substantial change in the resonant spectra in the intermediate state as in Fig. 5, though, the relative excitation efficiency of positive and negative gradient modes is reversed between the two. This is likely due to the collinearity of magnetization with the external field as we would expect parallel pumping to be inefficient when these are collinear.

As a whole, the trend we can take from the four experiments is that the resonant modes observed in the stripe domain phase are primarily determined by the pumping configuration. This is most stark for the bulk modes, the phase relationship of which is determined by the configuration. Mode hybridisation across the different edge and bulk sections is observed due to local exchange and dipole interactions. The good qualitative agreement of the simulated resonant spectra with the experimental ones demonstrate that, despite the discrepancy of the saturation field, the simulation parameters chosen still allow us to elucidate the origin of the resonant mode observed. At higher fields magnetic anisotropy determines the domain evolution in the ground state, on which different resonant modes are excited. This offers a potential

opportunity to enhance the reconfigurability of magnon systems by manipulation of the domain state.

### III. CONCLUSION AND OUTLOOK

We have studied the resonant spectra of the stripe domain state in  $3 \mu\text{m}$  thick LPE-grown YIG thin films. Due to its low damping, we resolved multiple spin-wave modes, where micro-magnetic simulations are a powerful tool to understand the spatial distribution of both static and dynamic components of magnetisation, e.g. modes populated in the flux closure caps and domain walls. We have shown how the small cubic anisotropy is able to dramatically affect the domain structure as a function of applied magnetic field and therefore the nature of resonant modes on the background magnetisation. The PMA present in our sample is extrinsic and as such, may be controlled by growth conditions e.g. growth direction in the case of growth-induced anisotropy [46, 47]. Application of strain [52, 53] or even spin currents [54] leads to potential opportunities for tuning this relatively weak anisotropy, realising reprogrammable magnonic modes excited on the stripe domain states. Observed resonances depending on the pumping geometry allow for another level of selectivity, controlled by small magnetic fields (1 - 4 mT) as demonstrated. This differentiates from other methods such as near infra-red pulses [55]. The stripe direction being influenced by the cubic anisotropy at zero field opens up another pathway to reorient these stripes and as such to change the excited resonances [56]. Our study is highly relevant to a recent study of magnetic stripes in  $\text{La}_{0.67}\text{Sr}_{0.33}\text{MnO}_3$ , exhibiting similar resonant and propagation modes tunable via stripe direction [57]. The ability to switch from a stripe domain state to com-

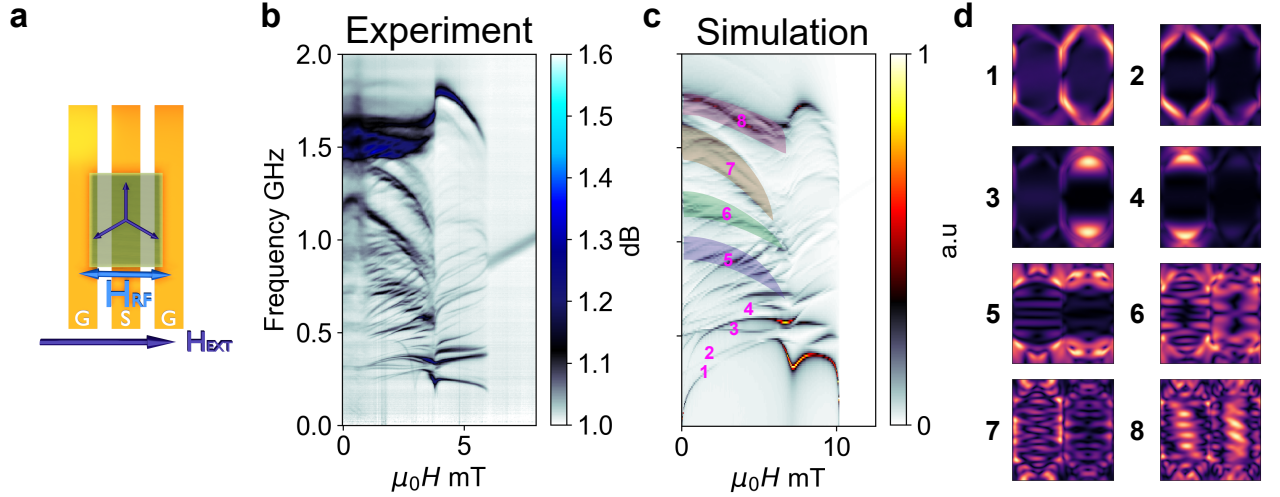


FIG. 6. a) Diagram showing the relative directions of external field, rf field and anisotropy axes. (b,c) Measured (b) and simulated (c) magnetic resonance spectra for YIG sample for rf  $\parallel \mathbf{H}_{\text{ext}}$  which is directed along the  $[11\bar{2}]$  axis. (d) power maps of spin wave modes labelled on (c)

pletely saturated state via the application of a relatively small field created an opportunity for multifunction devices that make use of both states for different purposes e.g. data processing and transfer.

### Appendix A: Simulation Parameters

We use mumax3 [49] to simulate the experimental results. To do this, we simulate a vertical section of the thin film with the height of the simulation set to the film thickness and the width to the stripe period. Periodic boundary conditions were then used to simulate the demagnetizing field. A schematic of the geometry is shown in Fig 2d. For the simulations, we used the anisotropy constants of  $K_u = 1000 \text{ Jm}^{-3}$  and  $K_c = -600 \text{ Jm}^{-3}$ . The  $K_c$  value is an approximate value from literature [58, 59], while the value is chosen to best reproduce the experimental results. This value is dramatically lower than the measured values previously provided, and even then the saturation field we see in simulation is approximately double that of the experiment. As the predominant source of anisotropy in our sample is the demagnetizing field, our method for calculating the uniaxial anisotropy involved subtracting the total anisotropy field from the demagnetizing field that we would expect for a thin film with the given measured value of  $M_s$ . Therefore, any error in the value of  $M_s$  has a much more significant

effect on the calculated  $K_u$ . As an example, a 2% change in the  $M_s$  value would lead to an over 35% change in  $K_u$ . In addition, for this calculation we approximate the shape to an infinitely thin plate. By doing this, the demagnetizing field is reduced to being uniform across the sample. This is not strictly speaking true as it would then directly cancel with the PMA and no stripes would form. This assumption provides a larger value for the demagnetizing field than it is in reality.

We also use an exchange stiffness value of  $6.5 \times 10^{-12} \text{ J/m}$  a value that is somewhat larger than the commonly reported value of  $\approx 4 \times 10^{-12} \text{ J/m}$  [60–62]. While for thin films the stripe domain width is typically equal to the film thickness,  $D$ , for thicker films the optimal width takes the form of

$$W_{\text{opt}} = 2\sqrt{2D\sqrt{A/K_{\perp}}}. \quad (\text{A1})$$

Using (A1) to calculate the optimal stripe domain width for the lower value gives  $W_{\text{opt}} = 1.23 \mu\text{m}$ , we then observe that even when the simulation is initiated with stripe domains of period  $1.5 \mu\text{m}$  as in the experiment, under applied field these domains will divide to produce a shorter domain width. While a value of  $9 \times 10^{-12} \text{ J/m}$  is required for  $W_{\text{opt}} = 1.5 \mu\text{m}$ , we choose  $6.5 \times 10^{-12} \text{ J/m}$  as a balance between these two options such that we do not see the division of the domains under applied field.

- 
- [1] A. V. Chumak, V. I. Vasyuchka, A. A. Serga, and B. Hillebrands, Magnon spintronics, *Nature Physics* **11**, 453 (2015).
  - [2] A. A. Serga, A. V. Chumak, and B. Hillebrands, YIG

magnonics, *Journal of Physics D: Applied Physics* **43**, 264002 (2010).

- [3] D. D. Awschalom, C. R. Du, R. He, F. J. Heremans, A. Hoffmann, J. Hou, H. Kurebayashi, Y. Li, L. Liu,

- V. Novosad, J. Sklenar, S. E. Sullivan, D. Sun, H. Tang, V. Tyberkevych, C. Trevillian, A. W. Tsen, L. R. Weiss, W. Zhang, X. Zhang, L. Zhao, and C. W. Zollitsch, Quantum engineering with hybrid magnonic systems and materials (invited paper), *IEEE Transactions on Quantum Engineering* **2**, 1 (2021).
- [4] B. Flebus, D. Grundler, B. Rana, Y. Otani, I. Barsukov, A. Barman, G. Gubbiotti, P. Landeros, J. Akerman, U. Ebels, P. Pirro, V. E. Demidov, K. Schultheiss, G. Csaba, Q. Wang, F. Ciubotaru, D. E. Nikonov, P. Che, R. Hertel, T. Ono, D. Afanasiev, J. Mentink, T. Rasing, B. Hillebrands, S. V. Kusminskiy, W. Zhang, C. R. Du, A. Finco, T. van der Sar, Y. K. Luo, Y. Shiota, J. Sklenar, T. Yu, and J. Rao, The 2024 magnonics roadmap, *Journal of Physics: Condensed Matter* **36**, 363501 (2024).
- [5] Y.-H. Rao, H.-W. Zhang, Q.-H. Yang, D.-N. Zhang, L.-C. Jin, B. Ma, and Y.-J. Wu, Liquid phase epitaxy magnetic garnet films and their applications\*, *Chinese Physics B* **27**, 086701 (2018).
- [6] R. Damon and H. van de Vaart, Dispersion of spin waves and magnetoelastic waves in YIG, *Proceedings of the IEEE* **53**, 348 (1965).
- [7] Y. Zhou, H. Jiao, Y.-t. Chen, G. E. W. Bauer, and J. Xiao, Current-induced spin-wave excitation in Pt/YIG bilayer, *Physical Review B* **88**, 184403 (2013).
- [8] B. Bhoi, T. Cliff, I. S. Maksymov, M. Kostylev, R. Aiyar, N. Venkataramani, S. Prasad, and R. L. Stamps, Study of photon-magnon coupling in a YIG-film split-ring resonant system, *Journal of Applied Physics* **116**, 243906 (2014).
- [9] L. J. Cornelissen, K. Oyanagi, T. Kikkawa, Z. Qiu, T. Kuschel, G. E. W. Bauer, B. J. van Wees, and E. Saitoh, Nonlocal magnon-polaron transport in yttrium iron garnet, *Physical Review B* **96**, 104441 (2017).
- [10] B. Satywali, V. P. Kravchuk, L. Pan, M. Raju, S. He, F. Ma, A. P. Petrović, M. Garst, and C. Panagopoulos, Microwave resonances of magnetic skyrmions in thin film multilayers, *Nature Communications* **12**, 1909 (2021).
- [11] K. Schultheiss, R. Verba, F. Wehrmann, K. Wagner, L. Körber, T. Hula, T. Hache, A. Kákay, A. A. Awad, V. Tiberkevich, A. N. Slavin, J. Fassbender, and H. Schultheiss, Excitation of whispering gallery magnons in a magnetic vortex, *Phys. Rev. Lett.* **122**, 097202 (2019).
- [12] K. Vogt, O. Sukhostavets, H. Schultheiss, B. Obry, P. Pirro, A. A. Serga, T. Sebastian, J. Gonzalez, K. Y. Guslienko, and B. Hillebrands, Optical detection of vortex spin-wave eigenmodes in microstructured ferromagnetic disks, *Phys. Rev. B* **84**, 174401 (2011).
- [13] J. C. Gartside, K. D. Stenning, A. Vanstone, H. H. Holder, D. M. Arroo, T. Dion, F. Caravelli, H. Kurebayashi, and W. R. Branford, Reconfigurable training and reservoir computing in an artificial spin-vortex ice via spin-wave fingerprinting, *Nature Nanotechnology* **17**, 460 (2022).
- [14] O. Lee, J. Sahliger, A. Aqeel, S. Khan, S. Seki, H. Kurebayashi, and C. H. Back, Tunable gigahertz dynamics of low-temperature skyrmion lattice in a chiral magnet, *Journal of Physics: Condensed Matter* **34**, 095801 (2021).
- [15] T. E. Hasty, Ferromagnetic resonance in multidomain thin films, *Journal of Applied Physics* **35**, 1434 (1964), <https://pubs.aip.org/aip/jap/article-pdf/35/5/1434/18331613/1434.1.online.pdf>.
- [16] R. Nakane, A. Hirose, and G. Tanaka, Spin waves propagating through a stripe magnetic domain structure and their applications to reservoir computing, *Physical Review Research* **3**, 033243 (2021).
- [17] O. Lee, T. Wei, K. D. Stenning, J. C. Gartside, D. Prestwood, S. Seki, A. Aqeel, K. Karube, N. Kanazawa, Y. Taguchi, C. Back, Y. Tokura, W. R. Branford, and H. Kurebayashi, Task-adaptive physical reservoir computing, *Nature Materials* **23**, 79 (2024).
- [18] A. Papp, W. Porod, and G. Csaba, Nanoscale neural network using non-linear spin-wave interference, *Nature Communications* **12**, 6422 (2021).
- [19] R. Nakane, G. Tanaka, and A. Hirose, Reservoir Computing With Spin Waves Excited in a Garnet Film, *IEEE Access* **6**, 4462 (2018).
- [20] B. Heinz, T. Brächer, M. Schneider, Q. Wang, B. Lägell, A. M. Friedel, D. Breitbach, S. Steinert, T. Meyer, M. Kewenig, C. Dubs, P. Pirro, and A. V. Chumak, Propagation of Spin-Wave Packets in Individual Nanosized Yttrium Iron Garnet Magnonic Conduits, *Nano Letters* **20**, 4220 (2020).
- [21] A. D. Giacco, F. Maspero, V. Levati, M. Vitali, E. Albisetti, D. Petti, L. Brambilla, V. Polewczyk, G. Vinai, G. Panaccione, R. Silvani, M. Madami, S. Tacchi, R. Dreyer, S. R. Lake, G. Woltersdorf, G. Schmidt, and R. Bertacco, Patterning Magnonic Structures via Laser Induced Crystallization of Yttrium Iron Garnet, *Advanced Functional Materials* **34**, 2401129 (2024).
- [22] M. Kiechle, A. Papp, S. Mendisch, V. Ahrens, M. Golibrzuch, G. H. Bernstein, W. Porod, G. Csaba, and M. Becherer, Spin-Wave Optics in YIG Realized by Ion-Beam Irradiation, *Small* **19**, 2207293 (2023).
- [23] D. Petti, S. Tacchi, and E. Albisetti, Review on magnonics with engineered spin textures, *Journal of Physics D: Applied Physics* **55**, 293003 (2022).
- [24] K. Szulc, S. Tacchi, A. Hierro-Rodríguez, J. Díaz, P. Gruszecki, P. Graczyk, C. Quirós, D. Markó, J. I. Martín, M. Vélez, D. S. Schmool, G. Carloti, M. Krawczyk, and L. M. Álvarez Prado, Reconfigurable Magnonic Crystals Based on Imprinted Magnetization Textures in Hard and Soft Dipolar-Coupled Bilayers, *ACS Nano* **16**, 14168 (2022).
- [25] K. Wagner, A. Kákay, K. Schultheiss, A. Henschke, T. Sebastian, and H. Schultheiss, Magnetic domain walls as reconfigurable spin-wave nanochannels, *Nature Nanotechnology* **11**, 432 (2016).
- [26] F. Garcia-Sanchez, P. Borys, R. Soucaille, J.-P. Adam, R. L. Stamps, and J.-V. Kim, Narrow Magnonic Waveguides Based on Domain Walls, *Physical Review Letters* **114**, 247206 (2015).
- [27] Y. Henry, D. Stoeffler, J.-V. Kim, and M. Bailleul, Unidirectional spin-wave channeling along magnetic domain walls of Bloch type, *Physical Review B* **100**, 024416 (2019).
- [28] R. B. Holländer, C. Müller, J. Schmalz, M. Gerken, and J. McCord, Magnetic domain walls as broadband spin wave and elastic magnetisation wave emitters, *Scientific Reports* **8**, 13871 (2018).
- [29] X. S. Wang and X. R. Wang, Spin wave emission in field-driven domain wall motion, *Physical Review B* **90**, 184415 (2014).
- [30] B. Van de Wiele, S. J. Hämäläinen, P. Baláz, F. Montoncello, and S. van Dijken, Tunable short-wavelength spin wave excitation from pinned magnetic domain walls, *Scientific Reports* **6**, 21330 (2016).



- [31] R. Salikhov, F. Samad, S. S. P. K. Arekapudi, R. Ehrler, J. Lindner, N. S. Kiselev, and O. Hellwig, Control and tunability of magnetic bubble states in multilayers with strong perpendicular magnetic anisotropy at ambient conditions, *Physical Review B* **106**, 054404 (2022).
- [32] A. Hubert and R. Schäfer, Domain Theory, in *Magnetic Domains: The Analysis of Magnetic Microstructures*, edited by A. Hubert and R. Schäfer (Springer, Berlin, Heidelberg, 1998) pp. 99–335.
- [33] S. Fin, R. Tomasello, D. Bisero, M. Marangolo, M. Sacchi, H. Popescu, M. Eddrief, C. Hepburn, G. Finocchio, M. Carpentieri, A. Rettori, M. G. Pini, and S. Tacchi, In-plane rotation of magnetic stripe domains in  $\text{Fe}_{1-x}\text{Ga}_x$  thin films, *Physical Review B* **92**, 224411 (2015).
- [34] W. Tee Soh, N. N. Phuoc, C. Y. Tan, and C. K. Ong, Magnetization dynamics in permalloy films with stripe domains, *Journal of Applied Physics* **114**, 053908 (2013).
- [35] I. S. Camara, S. Tacchi, L.-C. Garnier, M. Eddrief, F. Fortuna, G. Carlotti, and M. Marangolo, Magnetization dynamics of weak stripe domains in Fe–N thin films: a multi-technique complementary approach, *Journal of Physics: Condensed Matter* **29**, 465803 (2017).
- [36] N. Vukadinovic and J. B. Youssef, Nonlinear domain-mode ferromagnetic resonances in garnet films with perpendicular anisotropy, *Physical Review B* **100**, 224423 (2019).
- [37] B. Lührmann, H. Dötsch, and S. Sure, High-frequency excitations of stripe-domain lattices in magnetic garnet films, *Applied Physics A* **57**, 553 (1993).
- [38] M. Ramesh and P. E. Wigen, Ferromagnetodynamics of parallel stripe domains - domain walls system, *Journal of Magnetism and Magnetic Materials* **74**, 123 (1988).
- [39] U. Ebels, L. Buda, K. Ounadjela, and P. E. Wigen, Ferromagnetic resonance excitation of two-dimensional wall structures in magnetic stripe domains, *Physical Review B* **63**, 174437 (2001).
- [40] N. Vukadinovic, M. Labrune, J. B. Youssef, A. Marty, J. C. Toussaint, and H. Le Gall, Ferromagnetic resonance spectra in a weak stripe domain structure, *Physical Review B* **65**, 054403 (2001).
- [41] J. Wei, Z. Zhu, H. Feng, J. Du, Q. Liu, and J. Wang, Top-down control of dynamic anisotropy in permalloy thin films with stripe domains, *Journal of Physics D: Applied Physics* **48**, 465001 (2015).
- [42] A. V. Vashkovskii, E. G. Lokk, and V. I. Shcheglov, Propagation of magnetostatic waves in unsaturated ferrite films with a strip domain structure, *Journal of Experimental and Theoretical Physics* **84**, 560 (1997).
- [43] T. Kikkawa, K. Oyanagi, T. Hioki, M. Ishida, Z. Qiu, R. Ramos, Y. Hashimoto, and E. Saitoh, Composition-tunable magnon-polaron anomalies in spin Seebeck effects in epitaxial  $\text{Bi}_{1-x}\text{Y}_x\text{Fe}_{1-5x}\text{O}_{12}$  films, *Physical Review Materials* **6**, 104402 (2022).
- [44] O. Lee, K. Yamamoto, M. Umeda, C. W. Zollitsch, M. Elyasi, T. Kikkawa, E. Saitoh, G. E. W. Bauer, and H. Kurebayashi, Nonlinear Magnon Polaritons, *Physical Review Letters* **130**, 046703 (2023).
- [45] J. M. D. Coey, Nanoscale magnetism, in *Magnetism and Magnetic Materials* (Cambridge University Press, Cambridge, 2010) pp. 264–304.
- [46] W. T. Stacy and W. Tolksdorf, GROWTH-INDUCED MAGNETIC ANISOTROPY IN YTTRIUM IRON GARNET, *AIP Conference Proceedings* **5**, 185 (1972).
- [47] W. Ya-Qi and Z. Xun-Yi, Growth-induced magnetic anisotropy in YIG, *Hyperfine Interactions* **28**, 447 (1986).
- [48] E. Duda, B. Desormiere, and G. Volluet, Domain structure in YIG films subjected to magnetic fields and stresses, *IEEE Transactions on Magnetics* **10**, 634 (1974).
- [49] A. Vansteenkiste, J. Leliaert, M. Dvornik, M. Helsen, F. Garcia-Sanchez, and B. Van Waeyenberge, The design and verification of MuMax3, *AIP Advances* **4**, 107133 (2014).
- [50] C. Kittel, Theory of the Structure of Ferromagnetic Domains in Films and Small Particles, *Physical Review* **70**, 965 (1946).
- [51] J. M. D. Coey, Ferromagnetism and exchange, in *Magnetism and Magnetic Materials* (Cambridge University Press, Cambridge, 2010) pp. 128–194.
- [52] H. Wang, C. Du, P. C. Hammel, and F. Yang, Strain-tunable magnetocrystalline anisotropy in epitaxial  $\text{Y}_3\text{Fe}_5\text{O}_{12}$  thin films, *Physical Review B* **89**, 134404 (2014).
- [53] M. J. Gross, W. A. Misba, K. Hayashi, D. Bhattacharya, D. B. Gopman, J. Atulasimha, and C. A. Ross, Voltage modulated magnetic anisotropy of rare earth iron garnet thin films on a piezoelectric substrate, *Applied Physics Letters* **121**, 252401 (2022).
- [54] L. Chen, Y. Sun, S. Mankovsky, T. N. G. Meier, M. Kronseder, C. Sun, A. Orekhov, H. Ebert, D. Weiss, and C. H. Back, Signatures of magnetism control by flow of angular momentum, *Nature* **633**, 548 (2024).
- [55] M. Gidding, C. S. Davies, and A. Kirilyuk, Reorientation of magnetic stripe domains by mid-infrared pulses, *Physical Review B* **109**, L060408 (2024).
- [56] H. Yu, J. Xiao, and H. Schultheiss, Magnetic texture based magnonics, *Physics Reports Magnetic texture based magnonics*, **905**, 1 (2021).
- [57] Y. Zhang, L. Qiu, J. Chen, S. Wu, H. Wang, I. A. Malik, M. Cai, M. Wu, P. Gao, C. Hua, W. Yu, J. Xiao, Y. Jiang, H. Yu, K. Shen, and J. Zhang, Switchable long-distance propagation of chiral magnonic edge states, *Nature Materials* **24**, 69 (2025).
- [58] S. Lee, S. Grudichak, J. Sklenar, C. C. Tsai, M. Jang, Q. Yang, H. Zhang, and J. B. Ketterson, Ferromagnetic resonance of a YIG film in the low frequency regime, *Journal of Applied Physics* **120**, 033905 (2016).
- [59] P. Hansen, Anisotropy and magnetostriction of gallium-substituted yttrium iron garnet, *Journal of Applied Physics* **45**, 3638 (1974).
- [60] S. Klingler, A. V. Chumak, T. Mewes, B. Khodadadi, C. Mewes, C. Dubs, O. Surzhenko, B. Hillebrands, and A. Conca, Measurements of the exchange stiffness of YIG films using broadband ferromagnetic resonance techniques, *Journal of Physics D: Applied Physics* **48**, 015001 (2014).
- [61] J. C. Slonczewski, A. P. Malozemoff, and E. A. Giess, Temperature dependence of exchange stiffness in garnet bubble films, *Applied Physics Letters* **24**, 396 (1974).
- [62] K. Matsumoto, T. Brächer, P. Pirro, T. Fischer, D. Bozhko, M. Geilen, F. Heussner, T. Meyer, B. Hillebrands, and T. Satoh, Optical determination of the exchange stiffness constant in an iron garnet, *Japanese Journal of Applied Physics* **57**, 070308 (2018).